European Review for Medical and Pharmacological Sciences 2022; 26: 7918-7937

Technological advances in body CT: a primer for beginners

A. AGOSTINI[1,2], A. BORGHERESI[1], V. GRANATA[3], F. BRUNO[4], P. PALUMBO[5], F. DE MUZIO[6], E. BICCI[7], G. GRAZZINI[7], F. GRASSI[8], R. FUSCO[9], A. BARILE[2,4], V. MIELE[2,7], A. GIOVAGNONI[1]

[1]Department of Clinical, Special and Dental Sciences, University Politecnica delle Marche, Department of Radiology, University Hospital "Ospedali Riuniti Umberto I – G.M. Lancisi – G. Salesi", Ancona, Italy
[2]Italian Society of Medical and Interventional Radiology (SIRM), SIRM Foundation, Milan, Italy
[3]Division of Radiology, "Istituto Nazionale Tumori IRCCS Fondazione Pascale – IRCCS di Napoli", Naples, Italy
[4]Department of Biotechnological and Applied Clinical Sciences, University of L'Aquila, L'Aquila, Italy
[5]Department of Diagnostic Imaging, Abruzzo Health Unit 1, Area of Cardiovascular and Interventional Imaging, L'Aquila, Italy
[6]Department of Medicine and Health Sciences "V. Tiberio", University of Molise, Campobasso, Italy
[7]Department of Radiology, Careggi University Hospital, Florence, Italy
[8]Division of Radiology, Università Degli Studi Della Campania Luigi Vanvitelli, Naples, Italy
[9]Medical Oncology Division, Igea SpA, Naples, Italy

Abstract. – Many technological advances have entered the clinical routine of Computed Tomography (CT) imaging. The new CT scanners have specific solutions in gantry design to bear the mechanical solicitations. The X-ray tubes have been improved for faster acquisitions at low radiation exposure, while the innovations in CT detectors provide a better image quality. The optimization of image quality and contrast, and the reduction of radiation dose, cannot be achieved without the implementation of adequate reconstruction software, such as Iterative Reconstructions (IR) and Artificial Intelligence (AI). In recent years, dual-energy (DECT) technology has expanded the indications of CT.
In this narrative review, a panoramic overview of the technological novelties in CT imaging will be provided for optimal utilization of CT technology.

Introduction

Computed Tomography (CT) is a well-established and diffuse diagnostic tool with many indications and uses in body imaging, in acute or non-emergency settings. Since its introduction in the early 70s, many technological solutions have been introduced to improve diagnostic performance, to reduce motion artifacts and radiation exposure[1]. The new-generation scanners present several innovations in gantry design, X-ray tube, and detector technology[2]. These are coupled with significant innovations in software technology, from Iterative Reconstructions (IR) to Artificial Intelligence (AI), spectral imaging with dual-energy CT (DECT), and photon-counting CT[3-5]. Some of these solutions smoothly entered the clinical routine, while others are still under investigation; all of them must be understood for the optimal utilization of the newer CT scanners.

This narrative review will provide the principal highlights on the recent technologies in CT scanners with the main clinical applications. From the innovations in gantry design, X-ray tubes, and detectors, we will move to the novelties in reconstruction software and spectral CT.

Technical Advances: Gantry Design

The innovations in modern CT scanners are moving in two main directions: reduction of radiation dose and acquisition of scan volumes as wide as possible along the z-axis with a high temporal resolution[2,6].

During the last 10-15 years, detectors with an increasingly wider coverage on the z-axis (up to 192 to 320 detector rows and 16 cm coverage) have been introduced[1]. The possibility of the acquisition of an entire organ (e.g., the brain or the hearth) within a single rotation slowed the race for detectors with more slices and re-introduced the

Corresponding Author: Alessandra Borgheresi, MD; e-mail: alessandra.borgheresi@gmail.com

axial acquisitions both for dynamic contrast-enhanced studies (DCE), and to reduce the over-scanning[7,8].

The race for a better temporal resolution must involve rotation times. The goal of 0.20 s/rotation announced in 2014 has not been achieved and the fastest rotation speed is up to 0.28 s (Revolution CT, GE Healthcare, Milwaukee, Wisconsin) or 0.25 s (Somatom Force, Siemens Healthineers, Forchheim, Germany)[7,9]. The technical implementation of the gantry with such rotation speeds requires a specific design (e.g., friction-free air bearings and contactless data transfer) and must bear the tremendous centrifugal force which is up to 40 g at 0.25 s/rotation[1]. The centrifugal force of the gantry directly affects the cooling system of the X-ray tube, which necessitates a specific optimization, such as rotating envelope, convective cooling, and liquid bearings[1,10]. More recently, a specific cardiovascular scanner (CardioGraphe, GE Healthcare, Milwaukee, Wisconsin) achieved a rotation time of 0.24 thanks to the smaller gantry allowing a faster rotation speed at equal g-forces[2,11].

A fast-moving table (up to 74 cm/s with an acceleration of 150 cm/s^2) is necessary for ultrafast, high pitch (HP) acquisitions[12]. This is a particular acquisition technique of the dual-source scanners (TurboFlash, on Somatom Definition, Flash, Force, Siemens Healthineers, Forchheim, Germany) where acquisitions with pitch values of 3 are feasible with the double tube-detector system[13].

The latest innovations in gantry design involve the use of Artificial Intelligence (AI). Since the calibration of the scanner and the devices for dose reduction (e.g., the bow-tie filter and the current modulation, see below) assume that the patient is positioned at the isocenter, newer scanners mount an AI algorithm that automatically moves the patient to the isocenter under the guide of an infrared camera without centering errors[14,15].

Clinical Implementation in Body CT: Ultrafast Acquisitions

The main application of HP scans (TurboFlash, Siemens Healthineers, Forchheim, Germany) is in cardiovascular imaging[16]. Beyond it, the HP scans provided several advantages in the reduction of motion artifacts, particularly in chest scans. Lell et al[17] optimized a free-breathing, respiratory-triggered HP scan in uncooperative patients with satisfactory image quality, a significant reduction of motion artifacts, and a better delineation of anatomical structures when compared to standard CT acquisitions[17]. Comparable results were obtained with low dose protocols (LDCT) and in the COVID setting (Figure 1)[18,19]. It can be argued that a better depiction of anatomy does not match with diagnostic confidence: Braun et al[20] recorded satisfactory diagnostic performance in their study with HP protocol[20]. Gariani et al[21] assessed a cohort of adult patients undergoing thoracoabdominal CT for various clinical reasons[21]. The authors found comparable image quality between the standard CT (pitch 0.6) and dual-source HP scans (pitch 3.2) with significantly fewer motion artifacts in the latter[21]. These results were also confirmed in the emergency setting and in obese patients[22,23].

In pediatric CT, sedation can be required for young, uncooperative infants. Globally, HP protocols provide the best image quality and the most effective management of motion artifacts, without the need for general anesthesia or breath-hold acquisitions[24-26].

Technical Advances in Hardware: Tubes, Detectors, Modulation, and Filters

X-Ray Tubes

The main objectives of technological advances in X-ray tubes are reducing radiation exposure and optimizing contrast, short acquisitions, Z-axis coverage, and mechanical forces acting within the gantry[1].

Except for the last issue, the others are addressed by the improvement of tubes' output. First, the acquisitions at low kV allow for the reduction of radiation dose while optimizing the contrast enhancement (the mean energy of the beam gets closer to the K-edge of iodine) while the higher tube current compensates for the increased noise[27,28]. Second, the HP acquisitions require a consistently high output for short acquisition times[12]. Moreover, the tin filter mounted on some scanners (Somatom Flash and Force, Siemens Healthineers, Forchheim, Germany) for dose reduction (see below) absorbs up to 90% of the emitted photons; therefore, a high output is necessary for compensation[29,30]. Thus, the high-end X-ray tubes provide a wider choice of operating kV and a more powerful output at low voltages[31]. As an example, both the Vectron (Siemens Healthineers, Forchheim, Germany) and the Quantix 160 (GE

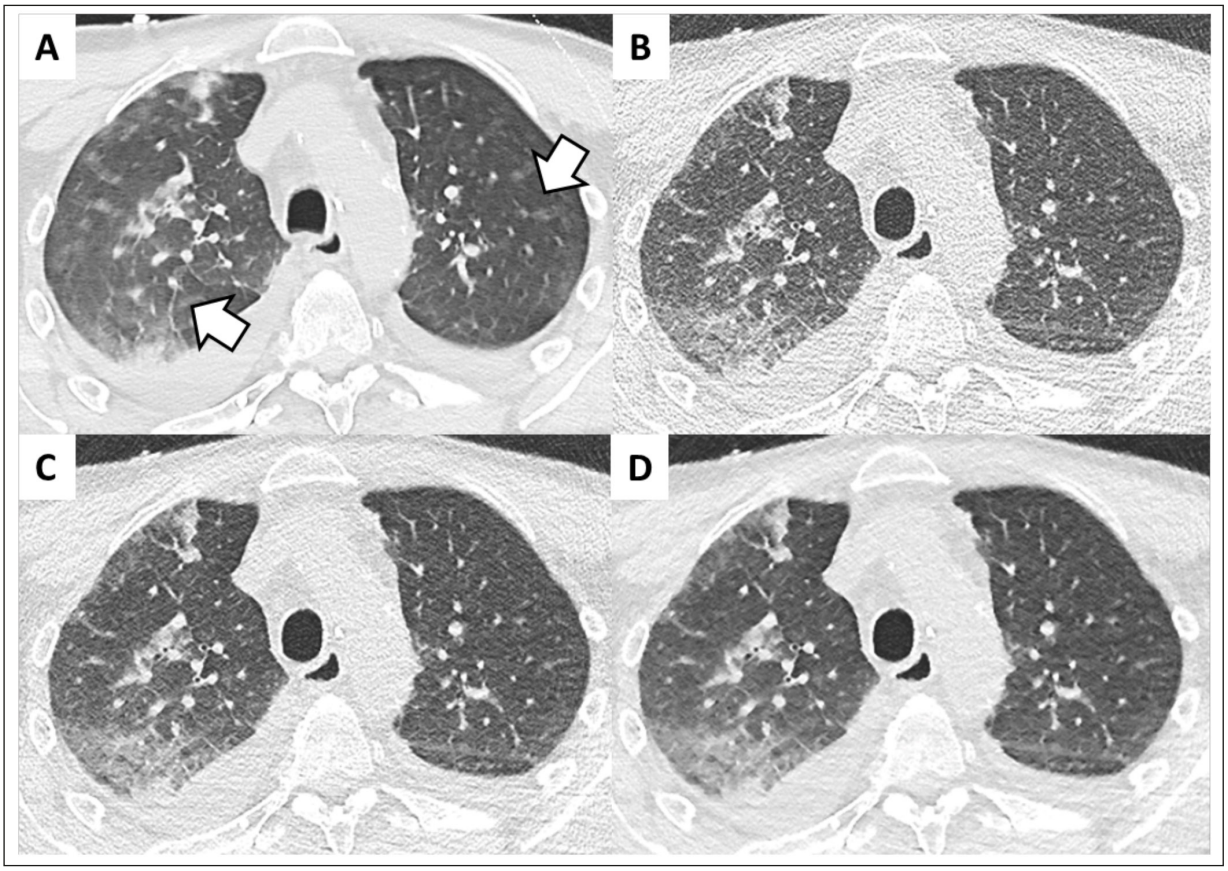

Figure 1. The role of high-pitch acquisition on a Dual-source CT (Somatom Force, Siemens Healthineers, Forchheim, Germany) with spectral shaping (tin filter). Uncooperative patient with COVID-19 (male, 77 y.o.). **A**, Dual-energy (DECT) acquisition (90/150Sn kV); rotation time: 0,25s, pitch: 1.1, exposure time: 1.98 s, ADMIRE 3. Radiation dose: CTDI 7.97 mGy; DLP: 381.5 mGycm. B-D. High-pitch acquisition (TurboFlash, Siemens Healthineers) with spectral shaping (100Sn kV); rotation time: 0,25 s, pitch 3, exposure time: 0.61 s, ADMIRE 0 (filtered backprojection). **B**, ADMIRE 3 (**C**), ADMIRE 5 (**D**). Radiation dose: CTDI 0.78 mGy; DLP: 30.5 mGycm. Image A is the acquisition at standard dose; the arrows point to the motion artifact due to cough. The high-pitch acquisition (images **B**-**D**) avoids the motion artifacts thanks to the rapid acquisition time. The reduction of radiation dose with the tin filter results in an exposure of 1/10 of the standard dose. The iterative reconstruction (ADMIRE) is fundamental for the optimization of image quality and adequate depiction of pulmonary structures (images **C** and **D**).

Healthcare, Milwaukee, Wisconsin) tubes deliver 1300 mA at 70 Kv; the Vectron tube has operating kV up to 150 kV, selectable in steps of 10 kV[32]. Third, the Z-axis coverage of the detector directly influences the cone angle of the X-ray beam, itself being proportional to the anode angle[33]. Consequently, an increased anode angle corresponds to a wider focal spot with a loss in spatial resolution. This can be compensated with a narrower electron beam leading to wear and cooling issues[34]. Among the high-end tubes, the Quantix 160 (GE Healthcare, Milwaukee, Wisconsin) has one of the higher anode angles (10°) for a collimation of 160 mm on the Z-axis[35]. Finally, these performances require a specific cooling design at high g-forces: specific examples are the rotating envelope and convective cooling (Straton or Vectron tubes, Siemens Healthineers), or the spiral groove where the liquid metal works as a bearing and cooling system[10,35,36].

Detectors

The recent advances in detector technology aim to improve the performance in terms of dose reduction, spatial resolution, and velocity of response[37]. A first strategy consists in the improvement of the electronics, namely the photodiode and the analog-to-digital converter, which contribute to image noise[31]. One of the recent advances is the integration of the photodiode and the converter in one integrated circuit (i.e., Stellar and Stellar Infinity detectors, Siemens Healthineers,

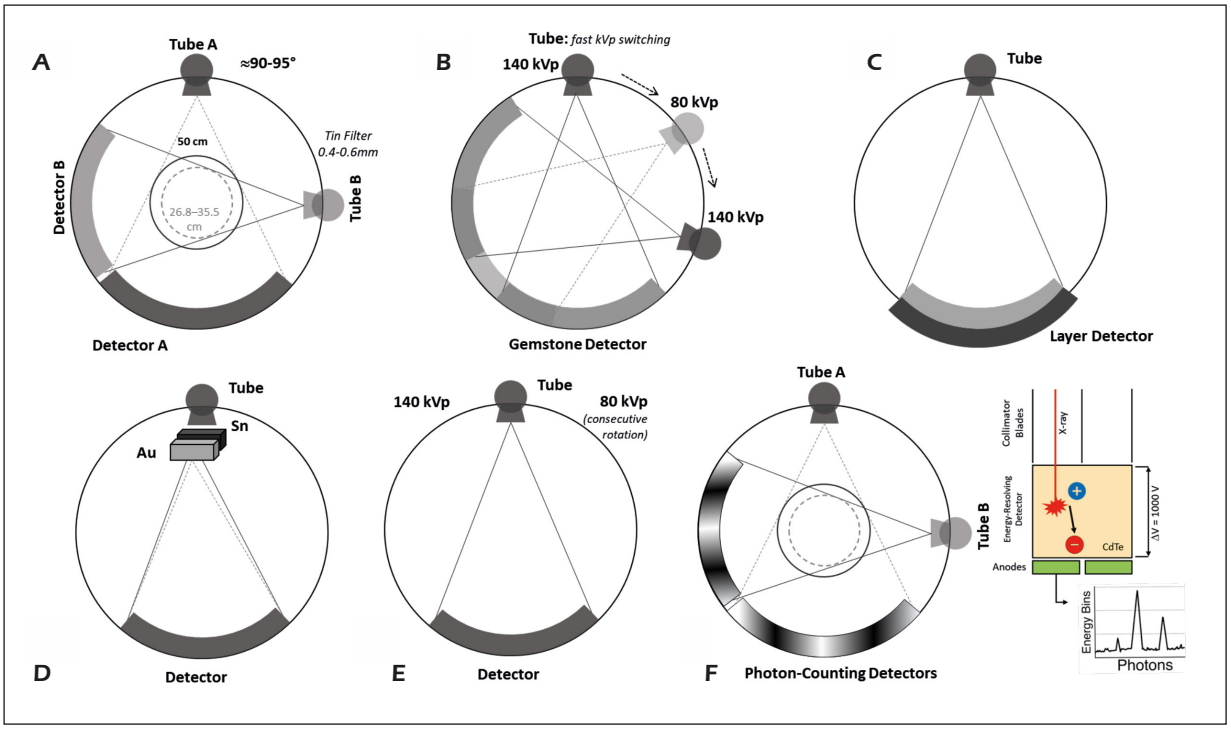

Figure 2. Spectral imaging: scanner design. **A**, Dual source (Siemens Healthineers, Forchheim, Germany). The two tube-detector systems are mounted with an offset of nearly 90°, increased in the latest generations to improve the Field of View of dual-energy acquisitions. Tube B, operating at high voltage in the 3rd generation scanner (140-150Sn kV), has the tin filter to improve the spectral separation. **B**, fast kVp switching (GE Healthcare, Milwaukee, Wisconsin). The X-ray tube has variable voltage while rotating (it switches between 80 and 140 kV). **C**, The layer detector (Philips Healthcare, Best, Netherlands) has two concentrical sensitive layers, the inner samples the low-energy photons, and the outer interacts with the higher part of the spectrum. **D**, Split Filter (Siemens Healthineers, Forchheim, Germany). The filter is composed by gold and tin components: these metals selectively cut the high and low components of the X-ray spectrum, thus splitting the beam. **E**, Consecutive acquisitions (Canon Medical Systems, Ōtawara, Japan). This strategy is usually implemented on scanners with wide coverage on the z-axis, the datasets are acquired sequentially with axial or helical mode. **F,** Photon-counting CT. The actual commercial solution (Naeotom Alpha, Siemens Healthineers, Forchheim, Germany) has a dual-source architecture. The crystals of CdTe of the energy-resolving detectors are in an electrical field of 800-1000 V. After the interaction, the electron migrates and produces an electrical pulse proportional to the incident X-ray photon energy.

Forchheim, Germany), with significant improvements in image quality in low-dose protocols or in obese patients[38,39].

The current technology of detectors is based on the indirect conversion of X-rays into electrical signals *via* visible light thanks to the scintillator materials[37]. The scintillator materials must fulfill several requirements: among the different materials, the Gd- oxysulfide is one of the most used[40-42]. More recently, other materials with better performance have been introduced[43]. For example, the garnet crystal (Gemstone Detector, GE Healthcare, Milwaukee, Wisconsin), has a primary decay time of 30 ns (100 times faster than Gd oxysulfide) and 25% of the afterglow of Gd oxysulfide; this material is fundamental for spectral imaging with fast kV switching (Figure 2 A-B)[44-46]. Other materials are available for spectral imaging[47]. The layer detector (IQon Spectral CT, Philips Healthcare) has a layer of ZnSe superimposed to a layer of Gd_2O_2S:Pr,Ce: the internal ZnSe layer is sensitive to and attenuates the low-energy photons, while the external layer is sensitive to the high-energy components of the spectrum (Figure 2 C-E)[48,49].

The energy-resolving detectors use semiconductors, such as cadmium-zinc-telluride (CZT), silicon (Si), or cadmium-telluride (CdTe) for direct conversion of the X-ray into electrical pulses[50-53]. The semiconductor is placed into an electric field (800-1000 V); the electron produced during the interaction with the X-ray photon is displaced and converted into the electrical signal proportional to the energy of the photon. Once the energy of the photons is quantified, they can be grouped into energy bins (Figure 2 F)[5]. This leads to several advantages in terms of image quality,

noise and dose reduction, multi-material decomposition, and spatial resolution[54-57].

Several solutions are useful to improve spatial resolution. First, smaller detector elements (from 0.625 mm to 0.25 mm, Aquilion Precision, Canon Medical Systems, Ōtawara, Japan) seem to provide a better spectral resolution; the use of an additional grid (Siemens Healthineers, Forchheim, Germany) is another strategy but is associated with higher radiation exposure[58,59].

Dose Reduction: Modulation of mA and kV

The automatic tube current modulation (ATCM) aims to homogenize the image noise through the different anatomical districts, which do not have a circular section nor a constant density[60,61]. Beyond the homogeneous image noise, the phantom and clinical studies showed a reduction of radiation exposure >50%[61,62].

The ACTM uses the scan projection image (SPI, scout view, or topogram) to calculate the size and the attenuation of the patient in one or two projections. The tube current is consequently modulated during the rotation in each quadrant or interpolated between the anteroposterior and lateral projections; the tube current is also modulated along the Z-axis[63,64]. The ATCM commonly works on image noise, which is managed differently by the available algorithms. However, the recognition of different structures relies on the contrast-to-noise ratio which depends on the patient's size and fat proportion: the ACTM algorithms can be optimized for higher image noise in larger patients[65,66]. For example, the CARE DOSE 4D (Siemens Healthineers, Forchheim, Germany) and DoseRight (Philips Healthcare, Best, Netherlands) use algorithms that increase the acceptable noise with the mean attenuation. In the first system, the reference tube current and the strength of modulation are manually selected[67]. The second has three modules: the automatic current modulation (manual or automatic), the longitudinal modulation (Z-DOM), and the angular modulation (D-DOM) working independently[68,69]. Conversely, in AutomA (GE Healthcare, Milwaukee, Wisconsin) and SURE EXPOSURE 3D (Canon Medical Systems, Ōtawara, Japan) algorithms, the operator chooses the noise level as a value of standard deviation in a standard phantom[70,71]. Further evolution of ATCM is the selective reduction of radiation exposure of superficial districts, such as the Organ Dose Modulation (GE Healthcare, Milwaukee, Wisconsin) or the X-CARE (Siemens Healthineers, Forchheim, Germany). These algorithms reduce the current when the tube irradiates superficial organs (e.g., breast or eyes) within variable angles of rotation (from 90° to 180°)[72,73].

With the availability of X-ray tubes with high power output and a wide range of operating kV, algorithms for automatic Voltage selection have been introduced, such as the kV Assist (GE Healthcare, Milwaukee, Wisconsin) or the CAREkV (Siemens Healthineers, Forchheim, Germany)[74,75]. These algorithms automatically select the optimal tube voltage and tube current with the lowest CTDI for the specific acquisition.

Beam Filtration and Spectral Shaping

In CT imaging, the energy spectrum of the emitted and measured X-rays at detectors are significantly different: this is known as the beam hardening effect[76]. The low-energy photons (<30 keV) are rapidly absorbed or scattered by the biological tissues: they contribute to the radiation dose while producing noise[76,77]. The beam hardening depends on the thickness of the tissue, which is lower at the lateral and peripheral portions of the body. The bowtie filters shape the X-ray beam: the variable thickness of the filter performs a more aggressive filtration of the peripheral sections of the X-ray beam with a reduction of the radiation exposure calculated in 10-20%[78].

The spectral shaping is a further strategy for dose reduction: a tin filter is added to the standard beam hardening filtration at the exit window of the X-ray tubes in dual-source scanners (Siemens Healthineers, Forchheim, Germany). The tin filter makes the X-ray beam narrower by selectively attenuating the quanta at lower energy levels; this leads to an increase of the mean energy of the beam with reduction of the beam hardening effect and significant reduction of radiation exposure[29,30].

Technical Advances in Software: Filtered Back Projection, Iterative Reconstruction, Artificial Intelligence

Together with hardware innovations for the reduction of radiation dose, several software solutions have been introduced to reduce the image noise and allow acquisitions with lower exposures[3]. For decades, the standard for image reconstructions in CT was the analytical method, the so-called filtered back projection (FBP)[79]. Considering the projections (raw data) of a hypothetical pencil beam measured by the detectors as an integral function of the angular and linear shift,

the FBP solves these equations by inversion and reconstructs the images; further evolution of the algorithm involves the fan beam and spiral acquisitions[79,80]. The FBP is associated with filters to compensate for the low-pass blur given by the different number of projections passing the object in the center and in the periphery: the higher the compensation, the higher the sharpness, the higher the spatial resolution and the image noise. The main strengths of FBP are the low complexity and low required computational power; however, the issues in the management of increasing noise prevent the reduction of radiation exposure with FBP (Figure 3, Table I)[81].

IR are algorithms that reduce the noise during the reconstruction process allowing for the reduction of radiation exposure. These algorithms work on the raw data or image domain and can be classified into statistical IR (hybrid), and model based IR[3].

From a theoretical point of view, IR consists of a stepwise, repeated calculation, where each step allows for updating or correction of a parameter until a defined criterion is matched. An ideal IR model involves forward and backward, repeated projection steps. Starting from a first image (e.g., estimated with FBP), synthetical raw data are calculated (forward projection) and compared with the measured raw data; the obtained correction parameter is propagated to the measured raw data for the estimation of an updated image (backward projection). The forward projection for the calculation of synthetic raw data requires models of the CT acquisition process: these are divided into CT system optics (related to the geometry of the gantry, the X-ray tube, and the detectors) and CT system statistics (related to the X-ray spectrum, the statistical distribution of photons and noise of the detector electronics) (Figure 3)[82].

Regarding the technological solutions, the hybrid IR uses separate filtration steps into raw data and/or image domain; the image reconstruction step relies on FBP. The filtration in the raw-data domain is a variation analysis to detect the noisy projections that will have a different weight for the final image reconstruction; in the image domain, the statistical models detect and filter the noise[83-86]. Even though the first statistical IR worked on the image domain (IRIS, Siemens Healthineers, Forchheim, Germany), the actual algorithms perform iterations on both domains[83,87,88]. The model-based IR involves at least one forward projection step; this step requires the system and optics model for the calculation of synthetical raw data and the update of the raw data at each iteration[89-91]. The main advantages of IR algorithms are the effective noise and dose reduction with acceptable image quality; when compared to FBP, the main drawbacks are the longer computational times and potential alteration of image texture (Figure 3, Table I)[89,92].

The altered image texture ("blotchy" or "oil painting") aspect of images is caused by the limitations of IR in the management of low-spatial-frequency noise and low-contrast spatial resolution at low radiation doses, due to the nonlinear relations between these parameters[92,93]. The AI algorithms have a different approach to overcome these issues. Machine Learning (ML) is a subgroup of AI that improves ("learns") its performances without specific programming: it can be classified into supervised (the data are labeled by humans and are used as ground truth during the training), unsupervised (the algorithm groups and separate using hidden parameters), and reinforcement learning (the algorithm works in a dynamic environment and receives feedback for positive or negative reinforcement)[94]. The Artificial Neural Networks (ANN) used in Deep Learning (DL) represent a subset of ML and have several connected modules (nodes or neurons) which simulate the human brain: the nodes are organized into an input layer, several hidden layers, and an output layer[95]. Among ANN, the convolutional neural networks (CNN) are suitable for image reconstruction: they are trained with low-dose, low-quality CT images and have as target data high-quality, high-dose images[96]. At present, two commercial solutions are available: the AiCE (Canon Medical Systems, Ōtawara, Japan) applies the CNN to improve the hybrid IR, while the TrueFidelity (GE Healthcare, Milwaukee, Wisconsin) directly reconstructs the images from projections (Figure 3)[97-99].

Clinical Implementation: Low Dose, Less Noise, High Contrast

One of the first applications of low-kV acquisitions with iterative reconstructions is the assessment of pulmonary embolism (PE)[100]. Knowing the average characteristics and comorbidities of patients with PE, the CT protocol is optimized for optimal intravascular contrast with the lowest dose of contrast material and associated reduction of radiation exposure[101,102]. The concomitant presence of other pulmonary pathologies, such as COVID-19 pneumonia, often requires specific adjustments for adequate evaluation of pulmonary parenchyma[103-106].

The implementation of low-dose CT protocols (LDCT, dose-length product (DLP) <1.5 mSv) in

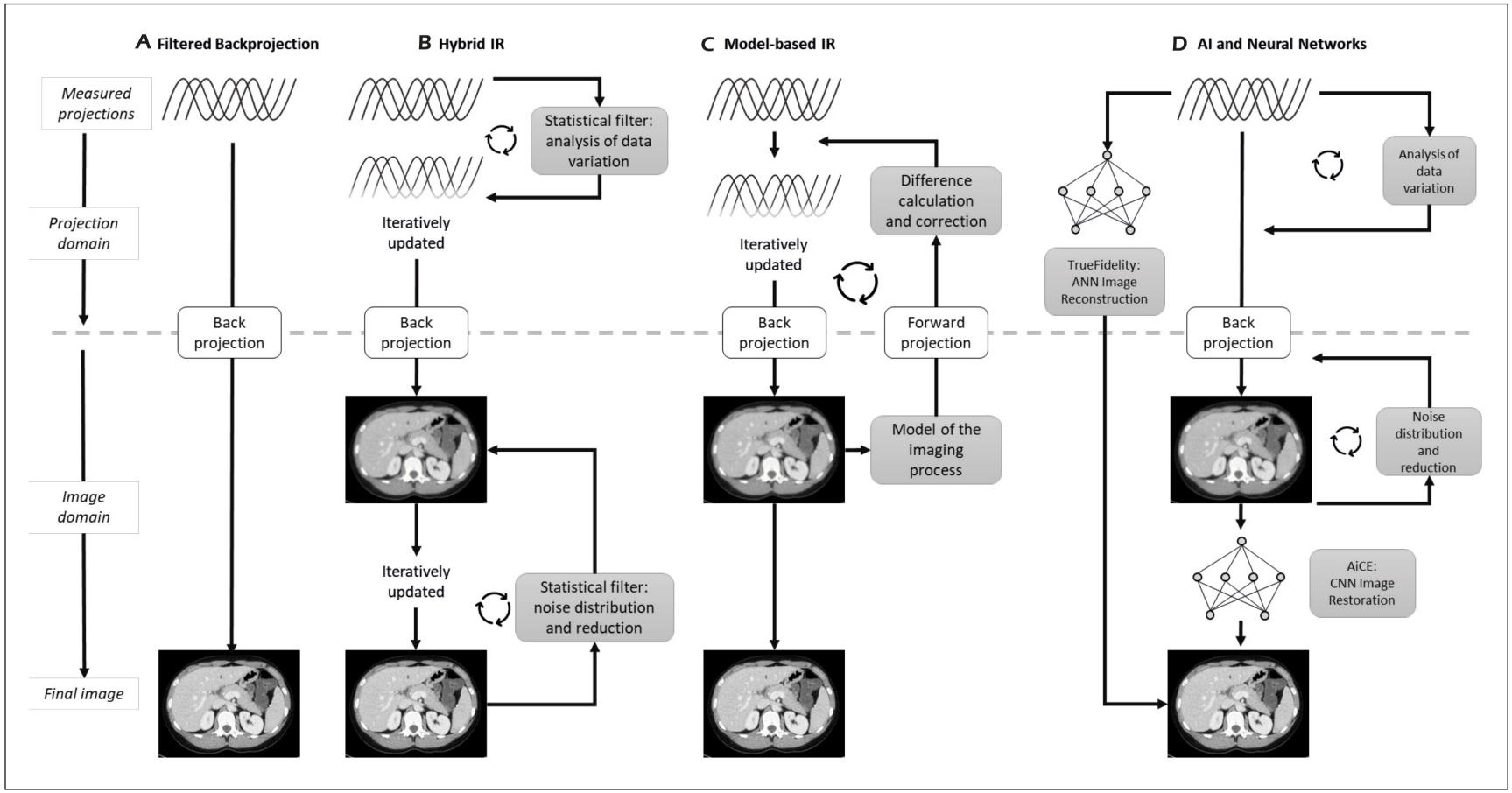

Figure 3. Image reconstruction in CT: (**A**) filtered back projection. **B**: Statistical (hybrid) Iterative Reconstruction (IR), **C**: Model-based IR, **D**: Artificial intelligence (AI) and Neural Networks. The Hybrid IR (**B**) involves at least one iteration cycle into the image or projection domain; most commercial solutions have iteration cycles in both domains. The Model-based IR algorithms (**C**) are characterized by at least one forward projection and involve complex models accounting for the acquisition process on the scanner. The two AI solutions (**D**) work differently: the AiCe (Canon Medical Systems, Otawara, Japan) has a neural network for image restoration after hybrid IR while the TrueFidelity (GE Healthcare, Milwaukee, Wisconsin) reconstructs the images from projections.

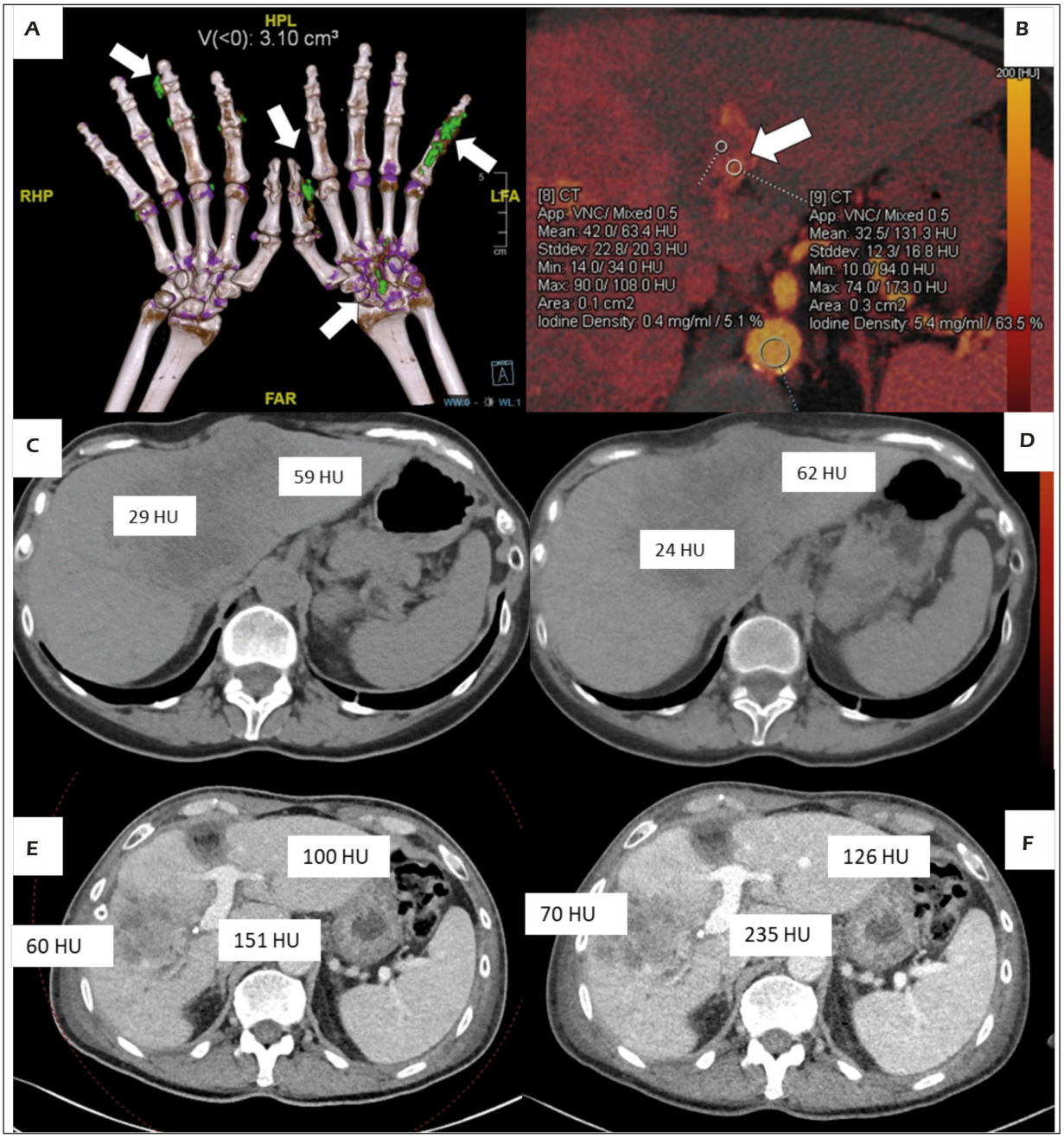

Figure 4. Dual-energy CT and material decomposition. **A-D**, Material-selective images. **C-D**, Energy-selective images. **A**, Material labeling. Patient with gout. The uric acid is labeled and colored in green (arrows) and the volume is quantified. **B**, Iodine map. The left portal branch has a mixed thrombus: the neoplastic component has a significantly higher iodine uptake (see labels in the image). **C-D**, Material subtraction and virtual non-contrast. **C,** basal acquisition at 120 kV. **D**, Virtual non-contrast (3rd generation dual-source CT, Somatom Force, 90/150Sn kV, Siemens Healthineers, Forchheim, Germany). Images **C** and **D** present comparable attenuations of the liver and the neoplastic lesion. **E,** 3rd generation dual-source CT, portal venous phase, 100/150Sn kV, Mixed 0.8. the blended image simulates the acquisition at 120 kV, the labels are the attenuation values of the liver lesion, the portal vein, and the liver. Image **F,** is the monochromatic reconstruction at 55 keV for magnification of image contrast, the labels are the attenuation of the same structures of image **E**.

Table I. Image Reconstruction in CT.

Reconstruction Technique	Acronyms	Strengths	Weaknesses
Filtered back projection	-	• Speed of reconstruction; • Control on image characteristics (e.g., kernel) • Image texture • Robustness of image metrics	• Image noise • Sensibility to artifacts (e.g., streaking) • Negligible dose reduction • Limited depiction of low-contrast objects
Hybrid (statistical) iterative reconstruction	**ASIR, ASIR-V** (Adaptive Statistical Iterative Reconstruction, GE Healthcare, Milwaukee, Wisconsin) **AIDR 3D** (Adaptive Iterative Dose Reduction 3D, Canon Medical Systems, Ōtawara, Japan) **iDose** (Philips Healthcare, Best, Netherlands) **SAFIRE** (Sinogram-affirmed iterative reconstruction, Siemens Healthineers, Forchheim, Germany)	• Noise reduction (moderate) • Resolution of low-contrast objects (moderate) • Dose reduction (moderate) • Artifact reduction (moderate)	• Speed of reconstruction; • Control on image characteristics • Oversmoothing; • Altered image texture • Robustness of image metrics
Model-based iterative reconstruction	**VEO** (MBIR, Model-Based Iterative Reconstruction, GE Healthcare, Milwaukee, Wisconsin) **FIRST** (Forward projected model-based Iterative Reconstruction Solution, Canon Medical Systems, Ōtawara, Japan) **IMR** (Iterative Model Reconstruction, Philips Healthcare, Best, Netherlands) **ADMIRE** (Advanced Modeled Iterative Reconstruction, Siemens Healthineers, Forchheim, Germany)	• Noise reduction (strong) • Resolution of low-contrast objects (moderate) • Dose reduction (strong) • Artifact reduction (strong)	• Speed of reconstruction; • Control on image characteristics • Oversmoothing; • Altered image texture • Robustness of image metrics
Artificial intelligence – Deep Learning Reconstruction	**AiCE** (Advanced intelligent Clear-IQ Engine, Canon Medical Systems, Ōtawara, Japan) **TrueFidelity** (GE Healthcare, Milwaukee, Wisconsin)	• Noise reduction (strong) • Resolution of low-contrast objects (strong) • Maintain spatial resolution (strong) • Artifact reduction (strong)	• Large training datasets accounting for personal differences; • Accurate selection of training data • Reduced sharpness of fine details (slight) • Robustness of image metrics

thoracic imaging is an active field of research, in particular with the introduction of lung-cancer screening campaigns[107]. The strategies for dose reduction depend on the scanner technology and are classified into the reduction of kV or mA, and the use of the tin filter[108]. In adult patients, the LDCT protocols on most scanners maintain a medium-high voltage (120 kV) with a significant reduction of tube current to maintain an acceptable image noise[109,110]. Conversely, in pediatric patients, the low voltages (e.g., 70 kV) have been successfully tested[111]. The IR has a pivotal role in the optimization of LDCT protocols in terms of noise and dose reduction; it has been estimated that at equal image quality, the IR reduces the dose by 26-50% in chest LDCT protocols[112]. These results are confirmed with both the hybrid and model based IR[29,113]. Most of the studies[108,113,114] with hybrid IR agree on the effective improvement of image quality, depiction of anatomical structures, and detection of pulmonary nodules. Some schol-

ars[115] highlighted potential lower conspicuity and diagnostic confidence in the low-contrast recognition tasks (e.g., ground-glass opacities) with hybrid IR; this finding has not been confirmed by all the studies with recommendations of prudential application of IR[113,116,117]. The model-based IR has the theoretical advantage of a lower influence on image texture; while some studies recorded better performances of model-based IR, others showed comparable diagnostic yield with the statistical IR[118-121].

Chest imaging is the main application of LDCT with the tin filter on the third-generation dual-source scanner (Siemens Healthineers, Forchheim, Germany)[29]. The proposed protocols, with spectral shaping, obtained a conspicuous reduction in radiation exposure (≈90%) with acceptable image quality and diagnostic performance[29,122,123]. The role of model-based IR (ADMIRE, Siemens Healthineers, Forchheim, Germany) is pivotal, and an optimal setting is required for the low-contrast recognition tasks (Figure 1)[123-125]. The technique has interesting applications in pediatric imaging, and it is usually coupled with high-pitch acquisitions[126]. Other preliminary reports[127-129] demonstrated the effectiveness of tin filter in abdominal studies, virtual colonography, or whole-body LDCT.

In abdominal studies[130], the CT protocols with low kV aim to improve the image contrast while reducing the radiation dose. Several reports demonstrated encouraging results in liver imaging for the detection of liver lesions[131,132], pancreatic tumors[133,134], the kidney and urinary tract[135,136], and for the assessment of the gastrointestinal tract[137,138]. The low-dose protocols are usually coupled with the use of IR for noise suppression and optimization of image quality[130-138]. Even if recommended, the IR demonstrated its limitations in the low-contrast recognition tasks, where the reduction of radiation dose depending on the IR is limited. In general, a reduction of radiation exposure >25% with stronger IR reconstruction leads to an altered image texture with significant degradation of diagnostic performance[139,140]. The use of DL for image reconstruction overcomes these limitations: the lesion detection and diagnostic performance are maintained at half radiation exposure [97,141].

Advanced CT Techniques: Spectral Imaging

The introduction of dual-energy CT (DECT) moved the frontiers of CT from morphology to function[142]. The material decomposition with DECT relies on the assumption that the attenuation of X-rays can be approximated to a linear combination of the Compton and the photoelectric effect, expressed as functions of material density and the energy of the X-ray beam[143,144]. This principle can be extended to a mixture of different materials: by scanning the same volume with two different X-ray spectra, it is possible to quantify two materials with known spectral curves[4]. With the inclusion of a third condition, such as the conservation of volume or mass, it is possible to include a third known material, to perform the three-material decomposition or multi-material decomposition[145]. The images obtained with the post-processing of DECT datasets provide several different information. Didactically, it is convenient to divide these images into material-selective (what kind of material am I assessing?) or energy-selective (what kind of information is the X-ray beam providing?)[47]. With material-selective images, a specific material (e.g., iodine) is detected (material labeling), quantified (e.g., quantitative maps or iodine maps), or subtracted (e.g., virtual non-contrast, VNC). With energy-selective images, the volume is scanned with a hypothetical monochromatic beam at different energy levels even not currently available on the scanner (i.e., monochromatic images); otherwise, information about the effective atomic number or effective density (rho-Z) can be extracted[146].

At present, several different technological solutions are commercially available for DECT scanners. Schematically, the spectral separation can be performed at the tube level or at the detector level. The first group includes the dual-source scanners with two tube-detector systems (the three generations of Somatom CT, Siemens Healthineers, Forchheim, Germany), the fast kV-switching (Revolution CT, GE Healthcare, Milwaukee, Wisconsin), the split filter (TwinBeam on Somatom Edge, Siemens Healthineers, Forchheim, Germany), and consecutive acquisitions (Aquilion One, Canon Medical Systems, Ōtawara, Japan). Two technologies are available for spectral separation at the detector level: the layer detector (IQon spectral CT, Philips Healthcare, Best, Netherlands) and the photon counting CT (Naeotom Alpha, Siemens Healthineers, Forchheim, Germany) (Figure 2)[147].

Each configuration has some advantages and disadvantages, as highlighted in Table II. The main advantage of the dual-source scanners (Siemens Healthineers, Forchheim, Germany) is the full control of the tube current and the spectral sepa-

Table II. Technological solutions for spectral imaging.

Scanner Technology	Models and Features	Strengths	Weaknesses
Dual Source	**Somatom Definition Flash, Drive, Force (Siemens Healthineers, Forchheim, Germany)** • Two independent tube-detector systems with an offset of ≈90°	• Full control on tubes' kV and mA • Highest spectral separation (tin filter) with robustness of material decomposition algorithms • Temporal resolution	• Maximum FOV for spectral information: 36 cm (adequate for most of body acquisitions) • Cross scattering • Spatial mismatch of the projections (≈90°) and image-space material decomposition
Fast kV switching	**Revolution CT (GE Healthcare, Milwaukee, Wisconsin)** • The X-ray tube switches the potential every 150 ms while rotating; • Detector with fast response	• Negligible mismatch pf projections (≈5°) allowing for • Projection-domain material decomposition and • Better beam hardening correction • Spectral information at full FOV of 50 cm	• Lower spectral separation • No tube current modulation requiring variable exposures at different energies • Limited rotation speed
Layer Detector	**IQon Spectral CT (Philips Healthcare, Best, Netherlands)** • Detector with two superimposed layers sensitive to different energies	• Simultaneous acquisition of the projections • Projection-domain material decomposition • Spectral information at full FOV of 50 cm	• Lower spectral separation and inaccurate material decomposition
Twin Beam	**TwinBeam on Somatom Edge (Siemens Healthineers, Forchheim, Germany)** • A filter with two different metals splits the X-ray beam int two spectra	• Potential easy implementation on current scanners	• Lower spectral separation and inaccurate material decomposition
Consecutive acquisitions	**Aquilion One (Canon Medical Systems, Ōtawara, Japan)** • Implemented only in scanners with wide z-coverage detectors	• Potentially absent mismatch of projections • Full control on tube kV and mA • Spectral information at full FOV of 50 cm	• Lowest temporal resolution: motion artifacts and inconsistencies between the datasets
Photon Counting	**Naeotom Alpha (Siemens Healthineers, Forchheim, Germany)** • Energy-resolving detectors quantifying and classifying the energy of each photon into bins	• Multi-energy imaging and multi-material decomposition; • Spectral information with high-pitch acquisitions in dual-source mode • Spatial resolution • Noise reduction • Dose reduction	• Image noise in multi-material decomposition

ration (i.e., the tube voltages), the latter is further improved by the tin filter thanks to the two independent tubes. Moreover, the scanner technology allows for fast acquisitions with an adequate temporal resolution[148]. Potential disadvantages are the cross scattering between the two tubes (specific software solutions have been introduced), the reduced FOV (up to 36 cm, adequate for almost all anatomical districts), and the DECT post-processing on the image domain due to the offset of projections[149]. In the fast kV switching (Revolution CT, GE Healthcare, Milwaukee, Wisconsin) the tube switches between two voltages while rotating: this requires specific features of the tube, the

generator (fast ramp-up between the two kVp), and detector (rapid response and short afterglow; Gemstone Detector, GE Healthcare, Milwaukee, Wisconsin). While the ATCM is not applicable and the spectral separation cannot be regulated, the DECT post-processing is performed on the projection domain at a full FOV of 50 cm[150]. The split filter (TwinBeam, Siemens Healthineers, Forchheim, Germany) uses a gold-tin filter to split the beam on the z-axis. It has a relatively easy implementation; conversely, it provides a relatively narrow spectral separation, but the DECT information is available at the full FOV of 50 cm[151]. Consecutive acquisitions are the first and oldest strategy applied and currently implemented on scanners with wide Z-axis coverage; the temporal mismatch may be a significant issue, but the DECT information is available at full FOV[147]. The two layers of layer detector (IQon Spectral, Philips Healthcare, Best, Netherlands) separate the high- and low-energy photons. However, the not-perfect separation reduces the spectral separation, but the DECT datasets are processed on the projection domain since they have an almost perfect spatial and temporal match[152].

The latest technology is the photon-counting detector (Naeotom Alpha, Siemens Healthineers, Forchheim, Germany), which is mounted on a dual-source architecture. Once the photons are detected and their energy is quantified, they are classified into energy bins. This allows for noise reduction (by selectively excluding specific bins), with consequent better spatial resolution and reduction of radiation dose. Moreover, the scanner architecture provides spectral data on HP acquisitions[153]. The photon-counting detector represents a significant evolution in spectral imaging: considering the energy bin as a separate X-ray spectrum, it is possible to perform the real multi-material decomposition with as many basis-materials as many energy bins are available[5,51].

Clinical Implementation: Spectral Imaging

The post-processing of DECT datasets must be optimized depending on the anatomical district and the available technology[4]. In general, each scanner technology provides different image series: for example, the dual-source scanners give blended images (i.e., a weighted average between the images from the two spectra), the fast switching provides a monochromatic series, and a 140 kV series as quality control, while the dual-layer uses a 120 kVp series[4,154]. Both the material- and energy-selective images are assessed in clinical practice: a general thoracoabdominal workflow involves monochromatic images (40-60 keV in thoracic studies for optimal contrast; 70 keV in abdominal studies to simulate the 120 kV) coupled with iodine maps (to assess the distribution of contrast material); further reconstructions are performed for specific clinical problems[154,155].

One of the main applications in thoracic imaging is the assessment of pulmonary embolism: the monochromatic images at low keV (40-60 keV) maximize the image contrast with reduced volumes of contrast material while the iodine maps highlight the perfusion defects of the lung parenchyma[156]. The use of iodine maps, and more specifically the lung PBV (Pulmonary Blood Volume, based on 3-material decomposition; Siemens Healthineers, Forchheim, Germany) goes beyond the pulmonary embolism, with promising results in the assessment of pulmonary lesions (e.g., characterization or evaluation of treatment response)[157,158], or diffuse diseases, such as emphysema, idiopathic pulmonary fibrosis but also in inflammatory lesions and COVID pneumonia[155,159-161].

Abdominal applications of DECT have been extensively evaluated (Figure 4 A, B). The main aim of virtual non-contrast images is the dose reduction by avoiding basal acquisition[13]; however, small differences in attenuation of abdominal parenchyma must be accounted (Figure 4 C, D)[162]. Monoenergetic images at low keV (40-55 keV) improve the visualization of hypervascular and hypovascular liver lesions (Figure 4 E, F)[163-165]; similar results were obtained in pancreatic adenocarcinoma[166]. Conversely, the monochromatic images at high energy (>100 keV) are useful for the reduction of beam-hardening artifacts, such as in metallic implants[167]. The qualitative or quantitative assessment of the iodine maps has several interesting applications in body imaging. Regarding the liver, the characterization of portal vein thrombus (Figure 4 B), the characterization and the assessment of treatment response of liver tumors, and the assessment of diffuse diseases, such as steatosis or iron overload, are interesting applications[168-172]. In pancreatic imaging, the iodine maps are useful for early diagnosis and parenchymal characterization in acute pancreatitis, while in genitourinary imaging the iodine maps allow for better characterization of renal cystic lesions[173,174]. The monochromatic images at low keV and the iodine maps have a complementary role in the assessment of the gastrointestinal tract and peritoneal compartment, in particular, for the characterization of inflammatory lesions (e.g., Crohn's disease), neoplastic lesions

(gastrointestinal or peritoneal localization), or vascular conditions (e.g., ischemia or bleeding)[154,175].

The material labeling and the rho-Z algorithms are often used in genitourinary or musculoskeletal imaging (Figure 4 A)[176-178]. In the characterization of urinary calculi, the CT numbers have several limitations, the most important being the overlap of HU values for the different materials[174]. The material labeling using the spectral curve of the uric acid allows for a significantly more accurate classification of urinary stones[179]. Similar algorithms are used for the assessment of urate crystals in gout with good diagnostic performance[180]. Another interesting application of material labeling is the virtual-non calcium images for the assessment of bone marrow edema from various causes[181,182]. The rho-Z algorithm provides information about the effective density and atomic number of the scanned mixture. More frequently it is used for the assessment of cartilages and tendons; however, ongoing studies are expanding the applications[146].

The photon counting technology is interesting for several reasons. The quanta responsible of image noise can be selectively subtracted by the detector with improved spatial resolution and reduction of radiation dose. Moreover, the X-ray photons can be accurately divided into several energy levels: this makes possible the real multi-material decomposition and K-edge imaging overcoming the limitations of DECT[51]. Finally, the currently available scanner (Naeotom Alpha, Siemens Healthineers) allows for the acquisition of spectral information with HP protocols[153].

Conclusions

The new technological solutions allow for better diagnostic performance and are expanding the indications of CT imaging. Adequate comprehension of these solutions allows for optimal utilization of the modern CT scanners.

Conflict of Interest

AA is a speaker for Siemens Healthineers. The other authors have no conflict of interest to disclose.

Ethical Approval

This review paper did not involve any human or animal subject and the ethical approval was not required.

Authors' Contribution

Literature search, wariting – original draft preparation, and manuscript editing: A.A., A. Bo., V.G., F.B., P.P., F.D.M., E.B., G.G., F.G., R.F. Manuscript editing and approval, and supervision: A. Ba, V.M., A.G. All authors have read and agreed to the published version of the manuscript. The authors confirm that the article is not under consideration for publication elsewhere. Each author has participated sufficiently to take public responsibility for the manuscript content.

ORCID ID

Andrea Agostini: https://orcid.org/0000-0002-0693-8257
Alessandra Borgheresi: https://orcid.org/0000-0002-5544-9468

References

1) Lell MM, Wildberger JE, Alkadhi H, Damilakis J, Kachelriess M. Evolution in Computed Tomography. Invest Radiol 2015; 50: 629-644.
2) Lell MM, Kachelrieß M. Recent and Upcoming Technological Developments in Computed Tomography: High Speed, Low Dose, Deep Learning, Multienergy. Invest Radiol 2020; 55: 8-19.
3) Willemink MJ, Noel PB. The evolution of image reconstruction for CT-from filtered back projection to artificial intelligence. Eur Radiol 2019; 29: 2185-2195.
4) McCollough CH, Leng S, Yu L, Fletcher JG. Dual- and Multi-Energy CT: Principles, Technical Approaches, and Clinical Applications. Radiology 2015; 276: 637-653.
5) Flohr T, Petersilka M, Henning A, Ulzheimer S, Ferda J, Schmidt B. Photon-counting CT review. Phys Medica 2020; 79: 126-136.
6) Masjedi H, Zare MH, Siahpoush NK, Razavi-Ratki SK, Alavi F, Shabani M. European trends in radiology: investigating factors affecting the number of examinations and the effective dose. Radiol Med 2020; 125: 296-305.
7) Liang J, Wang H, Xu L, Yang L, Dong L, Fan Z, Wang R, Sun Z. Diagnostic performance of 256-row detector coronary CT angiography in patients with high heart rates within a single cardiac cycle: a preliminary study. Clin Radiol 2017; 72: 694.e7-694.e14.
8) Lin L, Chen C, Tian H, Bivard A, Spratt N, Levi CR, Parsons MW. Perfusion Computed Tomography Accurately Quantifies Collateral Flow After Acute Ischemic Stroke. Stroke 2020; 51: 1006-1009.
9) Zhou Y, Hu L, Du S, Jin R, Li W, Lv F, Zhang Z. The ultrafast, high-pitch turbo FLASH mode of third-generation dual-source CT: Effect of different pitch and corresponding SFOV on image quality in a phantom study. J Appl Clin Med Phys 2021; 22: 158-167.
10) Schardt P, Deuringer J, Freudenberger J, Hell E, Knupfer W, Mattern D, Schild M. New x-ray tube performance in computed tomography by introducing the rotating envelope tube technology. Med Phy 2004; 31: 2699-2706.

11) Commandeur F, Goeller M, Dey D. Cardiac CT: Technological Advances in Hardware, Software, and Machine Learning Applications. Curr Cardiovasc Imaging Rep 2018; 11: 19.
12) Flohr TG, McCollough CH, Bruder H, Petersilka M, Gruber K, Suss C, Grasruck M, Stierstorfer K, Krauss B, Raupach R, Primak AN, Kuttner A, Achenbach S, Becker C, Kopp A, Ohnesorge BM. First performance evaluation of a dual-source CT (DSCT) system. Eur Radiol 2006; 16: 256-268.
13) Agostini A, Mari A, Lanza C, Schicchi N, Borgheresi A, Maggi S, Giovagnoni A. Trends in radiation dose and image quality for pediatric patients with a multidetector CT and a third-generation dual-source dual-energy CT. Radiol Med 2019; 124: 745-752.
14) Saltybaeva N, Schmidt B, Wimmer A, Flohr T, Alkadhi H. Precise and Automatic Patient Positioning in Computed Tomography. Invest Radiol 2018; 53: 641-646.
15) McCollough CH, Leng S. Use of artificial intelligence in computed tomography dose optimisation. Ann Icrp 2020; 49: 113-125.
16) Grutta LL, Toia P, Grassedonio E, Pasta S, Albano D, Agnello F, Maffei E, Cademartiri F, Bartolotta TV, Galia M, Midiri M. TAVI imaging: over the echocardiography. Radiol Med 2020; 125: 1148-1166.
17) Lell MM, Scharf M, Eller A, Wuest W, Allmendinger T, Fuchs F, Achenbach S, Uder M, May MS. Feasibility of Respiratory-gated High-pitch Spiral CT: Free-breathing Inspiratory Image Quality. Acad Radiol 2016; 23: 406-412.
18) Lim HK, Ha HI, Hwang HJ, Lee K. High-pitch, 120 kVp/30 mAs, low-dose dual-source chest CT with iterative reconstruction: Prospective evaluation of radiation dose reduction and image quality compared with those of standard-pitch low-dose chest CT in healthy adult volunteers. PLoS One 2019; 14: e0211097.
19) Agostini A, Floridi C, Borgheresi A, Badaloni M, Pirani PE, Terilli F, Ottaviani L, Giovagnoni A. Proposal of a low-dose, long-pitch, dual-source chest CT protocol on third-generation dual-source CT using a tin filter for spectral shaping at 100 kVp for CoronaVirus Disease 2019 (COVID-19) patients: a feasibility study. Radiol Med 2020; 125: 1-9.
20) Braun FM, Holzner V, Meinel FG, Armbruster M, Brandlhuber M, Ertl-Wagner B, Sommer WH. Improved assessment of mediastinal and pulmonary pathologies in combined staging CT examinations using a fast-speed acquisition dual-source CT protocol. Eur Radiol 2017; 27: 4931-4940.
21) Gariani J, Martin SP, Botsikas D, Becker CD, Montet X. Evaluating the effect of increased pitch, iterative reconstruction and dual source CT on dose reduction and image quality. Br J Radiology 2018; 91: 20170443.
22) Liang T, McLaughlin P, Arepalli CD, Louis LJ, Bilawich AM, Mayo J, Nicolaou S. Dual-source CT in blunt trauma patients: elimination of diaphragmatic motion using high-pitch spiral technique. Emerg Radiol 2016; 23: 127-132.
23) Forbrig R, Ingrisch M, Stahl R, Winter KS, Reiser M, Trumm CG. Radiation dose and image quality of high-pitch emergency abdominal CT in obese patients using third-generation dual-source CT (DSCT). Sci Rep 2019; 9: 15877.
24) Kino A, Zucker EJ, Honkanen A, Kneebone J, Wang J, Chan F, Newman B. Ultrafast pediatric chest computed tomography: comparison of free-breathing vs. breath-hold imaging with and without anesthesia in young children. Pediatr Radiol 2019; 49: 301-307.
25) Tivnan P, Winant AJ, Johnston PR, Plut D, Smith K, MacCallum G, Lee EY. Thoracic CTA in infants and young children: Image quality of dual-source CT (DSCT) with high-pitch spiral scan mode (turbo flash spiral mode) with or without general anesthesia with free-breathing technique. Pediatr Pulm 2021; 56: 2660-2667.
26) Lell MM, May M, Deak P, Alibek S, Kuefner M, Kuettner A, Köhler H, Achenbach S, Uder M, Radkow T. High-Pitch Spiral Computed Tomography. Invest Radiol 2011; 46: 116-123.
27) Aschoff AJ, Catalano C, Kirchin MA, Krix M, Albrecht T. Low radiation dose in computed tomography: the role of iodine. Br J Radiology 2017; 90: 20170079.
28) Silva M, Milanese G, Cobelli R, Manna C, Rasciti E, Poggesi S, Sverzellati N. CT angiography for pulmonary embolism in the emergency department: investigation of a protocol by 20 ml of high-concentration contrast medium. Radiol Med 2020; 125: 137-144.
29) Gordic S, Morsbach F, Schmidt B, Allmendinger T, Flohr T, Husarik D, Baumueller S, Raupach R, Stolzmann P, Leschka S, Frauenfelder T, Alkadhi H. Ultralow-dose chest computed tomography for pulmonary nodule detection: first performance evaluation of single energy scanning with spectral shaping. Invest Radiol 2014; 49: 465-473.
30) Primak AN, Giraldo JC, Eusemann CD, Schmidt B, Kantor B, Fletcher JG, McCollough CH. Dual-source dual-energy CT with additional tin filtration: Dose and image quality evaluation in phantoms and in vivo. AJR Am J Roentgenol 2010; 195: 1164-1174.
31) Ramirez-Giraldo J, Primak A, Grant K, Schmidt B, Fuld M. Radiation dose optimization technologies in multidetector computed tomography: a review. Med Phys Int 2014; 2: 420-430.
32) Meinel FG, Canstein C, Schoepf UJ, Sedlmaier M, Schmidt B, Harris BS, Flohr TG, Cecco CND. Image quality and radiation dose of low tube voltage 3rd generation dual-source coronary CT angiography in obese patients: a phantom study. Eur Radiol 2014; 24: 1643-1650.
33) Zink FE. X-ray tubes. Radiographics 1997; 17: 1259-1268.
34) Behling R, Hauttmann S, Holzarifel S, Marina W. P4–15: High Current X-Ray Source Technology for Medical Imaging. 2010 Ieee Int Vac Electron Conf Ivec 2010; 1: 475-476.
35) GE Healthcare. Revolution Apex. Published 2018. Accessed April 26, 2022. Available at: https://www.gehealthcare.com/products/computed-tomography/revolution-apex#powerful-platform
36) Schmidt T, Behling R. Maximus Rotalix Ceramic (MRC): a successful platform for future tube developments. Medica Mundi (Hamburg) 2001; 1: 50-55.
37) Shefer E, Altman A, Behling R, Goshen R, Gregorian L, Roterman Y, Uman I, Wainer N, Yagil Y,

Zarchin O. State of the Art of CT Detectors and Sources: A Literature Review. Curr Radiology Reports. 2013; 1: 76-91.
38) Morsbach F, Bickelhaupt S, Ratzer S, Schmidt B, Alkadhi H. Integrated circuit detector technology in abdominal CT: added value in obese patients. AJR Am J Roentgenol 2014; 202: 368-374.
39) Liu Y, Leng S, Michalak GJ, Vrieze TJ, Duan X, Qu M, Shiung MM, McCollough CH, Fletcher JG. Reducing image noise in computed tomography (CT) colonography: effect of an integrated circuit CT detector. J Comput Assist Tomogr 2014; 38: 398-403.
40) Yamada H, Suzuki A, Uchida Y, Yoshida M, Yamamoto H, Tsukuda Y. A Scintillator Gd2 O 2 S : Pr , Ce , F for X-Ray Computed Tomography. J Electrochem Soc 2019; 136: 2713-2716
41) Duclos SJ, Greskovich CD, Lyons RJ, Vartuli JS, Hoffman DM, Riedner RJ, Lynch MJ. Development of the HiLightTM scintillator for computed tomography medical imaging. Nucl Instruments Methods Phys Res Sect Accel Spectrometers Detect Assoc Equip 2003; 505: 68-71.
42) Eijk CW van. Inorganic scintillators in medical imaging. Phys Med Biol 2002; 47: R85-R106.
43) Melcher CL. Perspectives on the future development of new scintillators. Nucl Instruments Methods Phys Res Sect Accel Spectrometers Detect Assoc Equip 2005; 537: 6-14.
44) Kanai T, Satoh M, Miura I. Characteristics of a Nonstoichiometric Gd3+δ(Al,Ga)5–δO12:Ce Garnet Scintillator. J Am Ceram Soc 2008; 91: 456-462.
45) Vartuli J, Lyons R, Vess C, Mecvoy K, Hagerdon R, Duclos S, Nayak M, Jiang H. GE healthcare's new computed tomography scintillator - gemstone. In: 2008 Symposium on Radiation Measurements and Applications. Berkeley, CA, pp 2–5. Accessed June 14, 2021. Available at: https://www2.lbl.gov/Conferences/SORMA/assets/doc/SORMAOralProgram30May.pdf.
46) Zhang D, Li X, Liu B. Objective characterization of GE discovery CT750 HD scanner: gemstone spectral imaging mode. Med Phys 2011; 38: 1178-1188.
47) Cicero G, Ascenti G, Albrecht MH, Blandino A, Cavallaro M, D'Angelo T, Carerj ML, Vogl TJ, Mazziotti S. Extra-abdominal dual-energy CT applications: a comprehensive overview. Radiol Med 2020; 125: 384-397.
48) Brooks RA, Chiro GD. Split-detector computed tomography: a preliminary report. Radiology 1978; 126: 255-257.
49) Carmi R, Naveh G, Altman A. Material separation with dual-layer CT. In: IEEE Nuclear Science Symposium Conference Record, 2005: 1876-1878.
50) Overdick M, Bäumer C, Engel KJ, Fink J, Herrmann C, Krüger H, Simon M, Steadman R, Zeitler G. Towards Direct Conversion Detectors for Medical Imaging with X-Rays. 2008 Ieee Nucl Sci Symposium Conf Rec. Published online 2008: 1527-1535.
51) Willemink MJ, Persson M, Pourmorteza A, Pelc NJ, Fleischmann D. Photon-counting CT: Technical Principles and Clinical Prospects. Radiology 2018; 289: 293-312.
52) Fink J, Kraft E, Kruger H, Wermes N, Engel KJü, Herrmann C. Comparison of Pixelated CdZnTe, CdTe and Si Sensors With the Simultaneously Counting and Integrating CIX Chip. Ieee T Nucl Sci 2009; 56: 3819-3827.
53) Persson M, Huber B, Karlsson S, Liu X, Chen H, Xu C, Yveborg M, Bornefalk H, Danielsson M. Energy-resolved CT imaging with a photon-counting silicon-strip detector. Phys Med Biol 2014; 59: 6709-6727.
54) Symons R, Cork TE, Sahbaee P, Fuld MK, Kappler S, Folio LR, Bluemke DA, Pourmorteza A. Low-dose lung cancer screening with photon-counting CT: a feasibility study. Phys Med Biol 2016; 62: 202-213.
55) Zhou W, Montoya J, Gutjahr R, Ferrero A, Halaweish A, Kappler S, McCollough C, Leng S. Lung nodule volume quantification and shape differentiation with an ultra-high resolution technique on a photon-counting detector computed tomography system. J Medical Imaging 2017; 4: 043502.
56) Nasirudin RA, Mei K, Penchev P, Panchev P, Fehringer A, Pfeiffer F, Rummeny EJ, Fiebich M, Noël PB. Reduction of Metal Artifact in Single Photon-Counting Computed Tomography by Spectral-Driven Iterative Reconstruction Technique. PLoS One 2015; 10: e0124831.
57) Ferda J, Vendiš T, Flohr T, Schmidt B, Henning A, Ulzheimer S, Pecen L, Ferdová E, Baxa J, Mírka H. Computed tomography with a full FOV photon-counting detector in a clinical setting, the first experience. Eur J Radiol 2021; 137: 109614.
58) Meyer M, Haubenreisser H, Raupach R, Schmidt B, Lietzmann F, Leidecker C, Allmendinger T, Flohr T, Schad LR, Schoenberg SO, Henzler T. Initial results of a new generation dual source CT system using only an in-plane comb filter for ultra-high resolution temporal bone imaging. Eur Radiol 2015; 25: 178-185.
59) Baek J, Pineda AR, Pelc NJ. To bin or not to bin? The effect of CT system limiting resolution on noise and detectability. Phys Med Biol 2013; 58: 1433-1446.
60) Gies M, Kalender WA, Wolf H, Suess C, Madsen MT. Dose reduction in CT by anatomically adapted tube current modulation. I. Simulation studies. Med Phys 1999; 26: 2235-2247.
61) Kalender WA, Wolf H, Suess C. Dose reduction in CT by anatomically adapted tube current modulation. II. Phantom measurements. Med Phys 1999; 26: 2248-2253.
62) Greess H, Wolf H, Baum U, Lell M, Pirkl M, Kalender W, Bautz WA. Dose reduction in computed tomography by attenuation-based on-line modulation of tube current: evaluation of six anatomical regions. Eur Radiol 2000; 10: 391-394.
63) Lee CH, Goo JM, Ye HJ, Ye SJ, Park CM, Chun EJ, Im JG. Radiation Dose Modulation Techniques in the Multidetector CT Era: From Basics to Practice1. Radiographics 2008; 28: 1451-1459.
64) Martin CJ, Sookpeng S. Setting up computed tomography automatic tube current modulation systems. J Radiol Prot 2016; 36: R74.
65) Sookpeng S, Martin CJ, Gentle DJ, Lopez-Gonzalez MR. Relationships between patient size, dose and image noise under automatic tube current modulation systems. J Radiol Prot 2013; 34: 103-123.

66) Wilting JE, Zwartkruis A, Leeuwen MS van, Timmer J, Kamphuis AG, Feldberg M. A rational approach to dose reduction in CT: individualized scan protocols. Eur Radiol 2001; 11: 2627-2632.
67) Söderberg M. Overview, practical tips and potential pitfalls of using automatic exposure control in CT: Siemens CARE DOSE 4D. Radiat Prot Dosim 2015; 169: 84-91.
68) Stratis A, Kottou S, Molfetas M, Xirafi I, Delis H, Panayiotakis G. The effect of a combined tube current modulation system on dose delivered to patients undergoingthoracic and abdominal CT with a 128-slice scanner. Radiat Prot Dosim 2012; 153: 206-211.
69) Wood TJ, Moore CS, Stephens A, Saunderson JR, Beavis AW. A practical method to standardise and optimise the Philips DoseRight 2.0 CT automatic exposure control system. J Radiol Prot 2015; 35: 495.
70) Moro L, Panizza D, D'Ambrosio D, Carne I. Considerations on an automatic computed tomography tube current modulation system. Radiat Prot Dosim 2013; 156: 525-530.
71) Gombolevskiy V, Morozov S, Chernina V, Blokhin I, Vassileva J. A phantom study to optimise the automatic tube current modulation for chest CT in COVID-19. European Radiology Exp 2021; 5: 21.
72) Dixon MT, Loader RJ, Stevens GC, Rowles NP. An evaluation of organ dose modulation on a GE Optima CT660-computed tomography scanner. J Appl Clin Med Phys 2016; 17: 380-391.
73) Hoang JK, Yoshizumi TT, Choudhury KR, Nguyen GB, Toncheva G, Gafton AR, Eastwood JD, Lowry C, Hurwitz LM. Organ-Based Dose Current Modulation and Thyroid Shields: Techniques of Radiation Dose Reduction for Neck CT. AJR Am J Roentgenol 2012; 198: 1132-1138.
74) Spearman JV, Schoepf UJ, Rottenkolber M, Driesser I, Canstein C, Thierfelder KM, Krazinski AW, Cecco CND, Meinel FG. Effect of Automated Attenuation-based Tube Voltage Selection on Radiation Dose at CT: An Observational Study on a Global Scale. Radiology 2016; 279: 167-174.
75) Li M, Feng S, Wu N, Zhang L. Scout-Based Automated Tube Potential Selection Technique (kV Assist) in Enhanced Chest Computed Tomography. J Comput Assist Tomogr 2017; 41: 442-445.
76) Brooks RA, Chiro GD. Beam hardening in X-ray reconstructive tomography. Phys Med Biol 1976; 21: 390-398.
77) Boas FE, Fleischmann D. CT artifacts: causes and reduction techniques. Imaging Medicine 2012; 4: 229-240.
78) McCollough CH, Primak AN, Saba O, Bruder H, Stierstorfer K, Raupach R, Suess C, Schmidt B, Ohnesorge BM, Flohr TG. Dose performance of a 64-channel dual-source CT scanner. Radiology 2007; 243: 775-784.
79) Feldkamp L, Davis L, Kress J. Practical cone-beam algorithm. Josa. 1984; 1: 612-619.
80) Kudo H, Noo F, Defrise M. Cone-beam filtered-backprojection algorithm for truncated helical data. Phys Med Biol 1998; 43: 2885-2909.
81) Geyer LL, Schoepf UJ, Meinel FG, W. JrN J, Bastarrika G, Leipsic JA, Paul NS, Rengo M, Laghi A, De Cecco CN. State of the Art: Iterative CT Reconstruction Techniques. Radiology 2015; 276: 339-357.
82) Mehta D, Thompson R, Morton T, Dhanantwari A, E S. Iterative model reconstruction: simultaneously lowered computed tomography radiation dose and improved image quality. Med Phys Int 2013; 2: 147-155.
83) Willemink MJ, Jong PA de, Leiner T, Heer LM de, Nievelstein RA, Budde RP, Schilham AM. Iterative reconstruction techniques for computed tomography Part 1: technical principles. Eur Radiol 2013; 23: 1623-1631.
84) Noel PB, Fingerle AA, Renger B, Munzel D, Rummeny EJ, Dobritz M. Initial performance characterization of a clinical noise-suppressing reconstruction algorithm for MDCT. AJR Am J Roentgenol 2011; 197: 1404-1409.
85) Singh S, Kalra MK, Gilman MD, Hsieh J, Pien HH, Digumarthy SR, Shepard JA. Adaptive statistical iterative reconstruction technique for radiation dose reduction in chest CT: a pilot study. Radiology 2011; 259: 565-573.
86) Winklehner A, Karlo C, Puippe G, Schmidt B, Flohr T, Goetti R, Pfammatter T, Frauenfelder T, Alkadhi H. Raw data-based iterative reconstruction in body CTA: evaluation of radiation dose saving potential. Eur Radiol 2011; 21: 2521-2526.
87) Tipnis S, Ramachandra A, Huda W, Hardie A, Schoepf J, Costello P, Flohr T, Sedlmair M. Iterative reconstruction in image space (IRIS) and lesion detection in abdominal CT. P Soc Photo-opt Ins. Published online 2010 :76222K-76222K - 12.
88) Cristofaro M, Rizzi EB, Piselli P, Pianura E, Petrone A, Fusco N, Stefano FD, Schinina' V. Image quality and radiation dose reduction in chest CT in pulmonary infection. Radiol Med 2020; 125: 451-460.
89) Stiller W. Basics of iterative reconstruction methods in computed tomography: A vendor-independent overview. Eur J Radiol 2018; 109: 147-154.
90) Choi SJ, Park SH, Shim YS, Hwang JH, Park S, Pak SY, You MW, Park SH. Comparison of image quality and focal lesion detection in abdominopelvic CT: Potential dose reduction using advanced modelled iterative reconstruction. Clin Imag 2020; 62: 41-48.
91) Moloney F, James K, Twomey M, Ryan D, Grey TM, Downes A, Kavanagh RG, Moore N, Murphy MJ, Bye J, Carey BW, McSweeney SE, Deasy C, Andrews E, Shanahan F, Maher MM, O'Connor OJ. Low-dose CT imaging of the acute abdomen using model-based iterative reconstruction: a prospective study. Emerg Radiology 2019; 26: 169-177.
92) Mileto A, Guimaraes LS, McCollough CH, Fletcher JG, Yu L. State of the Art in Abdominal CT: The Limits of Iterative Reconstruction Algorithms. Radiology 2019; 293: 491-503.
93) McCollough CH, Yu L, Kofler JM, Leng S, Zhang Y, Li Z, Carter RE. Degradation of CT Low-Contrast Spatial Resolution Due to the Use of Iterative Reconstruction and Reduced Dose Levels. Radiology 2015; 276: 499-506.
94) Deo RC. Machine Learning in Medicine. Circulation 2015; 132: 1920-1930.
95) LeCun Y, Bengio Y, Hinton G. Deep learning. Nature. 2015; 521:436-444.

96) Chen H, Zhang Y, Kalra MK, Lin F, Chen Y, Liao P, Zhou J, Wang G. Low-Dose CT With a Residual Encoder-Decoder Convolutional Neural Network. Ieee T Med Imaging 2017; 36: 2524-2535.
97) Nakamura Y, Higaki T, Tatsugami F, Zhou J, Yu Z, Akino N, Ito Y, Iida M, Awai K. Deep Learning–based CT Image Reconstruction: Initial Evaluation Targeting Hypovascular Hepatic Metastases. Radiology Artif Intell 2019; 1: e180011.
98) Racine D, Brat HG, Dufour B, Steity JM, Hussenot M, Rizk B, Fournier D, Zanca F. Image texture, low contrast liver lesion detectability and impact on dose: Deep learning algorithm compared to partial model-based iterative reconstruction. Eur J Radiol 2021; 141: 109808.
99) Sun J, Li H, Gao J, Li J, Li M, Zhou Z, Peng Y. Performance evaluation of a deep learning image reconstruction (DLIR) algorithm in "double low" chest CTA in children: a feasibility study. Radiol Med 2021; 126: 1181-1188.
100) Ippolito D, Vito AD, Franzesi CT, Riva L, Pecorelli A, Corso R, Crespi A, Sironi S. Evaluation of image quality and radiation dose saving comparing knowledge model–based iterative reconstruction on 80-kV CT pulmonary angiography (CTPA) with hybrid iterative reconstruction on 100-kV CT. Emerg Radiology 2019; 26: 145-153.
101) Cozzi D, Moroni C, Cavigli E, Bindi A, Caviglioli C, Nazerian P, Vanni S, Miele V, Bartolucci M. Prognostic value of CT pulmonary angiography parameters in acute pulmonary embolism. Radiol Med 2021; 126: 1030-1036.
102) Sauter A, Koehler T, Fingerle AA, Brendel B, Richter V, Rasper M, Rummeny EJ, Noël PB, Münzel D. Ultra Low Dose CT Pulmonary Angiography with Iterative Reconstruction. PLoS One 2016; 11: e0162716.
103) Cavagna E, Muratore F, Ferrari F. Pulmonary Thromboembolism in COVID-19: Venous Thromboembolism or Arterial Thrombosis? Radiology Cardiothorac Imaging 2020; 2: e200289.
104) Ippolito D, Giandola T, Maino C, Pecorelli A, Capodaglio C, Ragusi M, Porta M, Gandola D, Masetto A, Drago S, Allegranza P, Corso R, Franzesi CT, Sironi S. Acute pulmonary embolism in hospitalized patients with SARS-CoV-2-related pneumonia: multicentric experience from Italian endemic area. Radiol Med 2021; 126: 1-10.
105) Riyahi S, Dev H, Behzadi A, Kim J, Attari H, Raza SI, Margolis DJ, Jonisch A, Megahed A, Bamashmos A, Elfatairy K, Prince MR. Pulmonary Embolism in Hospitalized Patients with COVID-19: A Multicenter Study. Radiology 2021; 301: E426-E433.
106) Masselli G, Almberger M, Tortora A, Capoccia L, Dolciami M, D'Aprile MR, Valentini C, Avventurieri G, Bracci S, Ricci P. Role of CT angiography in detecting acute pulmonary embolism associated with COVID-19 pneumonia. Radiol Med 2021; 126: 1553-1560.
107) Jonas DE, Reuland DS, Reddy SM, Nagle M, Clark SD, Weber RP, Enyioha C, Malo TL, Brenner AT, Armstrong C, Coker-Schwimmer M, Middleton JC, Voisin C, Harris RP. Screening for Lung Cancer With Low-Dose Computed Tomography. JAMA 2021; 325: 971-987.
108) Hammond E, Sloan C, Newell JD, Sieren JP, Saylor M, Vidal C, Hogue S, Stefano FD, Sieren A, Hoffman EA, Sieren JC. Comparison of low- and ultralow-dose computed tomography protocols for quantitative lung and airway assessment. Med Phys 2017; 44: 4747-4757.
109) Khawaja RDA, Singh S, Madan R, Sharma A, Padole A, Pourjabbar S, Digumarthy S, Shepard JA, Kalra MK. Ultra low-dose chest CT using filtered back projection: Comparison of 80-, 100- and 120kVp protocols in a prospective randomized study. Eur J Radiol 2014; 83: 1934-1944.
110) Rampado O, Depaoli A, Marchisio F, Gatti M, Racine D, Ruggeri V, Ruggirello I, Darvizeh F, Fonio P, Ropolo R. Effects of different levels of CT iterative reconstruction on low-contrast detectability and radiation dose in patients of different sizes: an anthropomorphic phantom study. Radiol Med 2021; b126: 55-62.
111) Niemann T, Henry S, Duhamel A, Faivre JB, Deschildre A, Colas L, Santangelo T, Remy J, Remy-Jardin M. Pediatric chest CT at 70 kVp: a feasibility study in 129 children. Pediatr Radiol 2014; 44: 1347-1357.
112) Klink T, Obmann V, Heverhagen J, Stork A, Adam G, Begemann P. Reducing CT radiation dose with iterative reconstruction algorithms: The influence of scan and reconstruction parameters on image quality and CTDIvol. Eur J Radiol 2014; 83: 1645-1654.
113) Kim Y, Kim YK, Lee BE, Lee SJ, Ryu YJ, Lee JH, Chang JH. Ultra-Low-Dose CT of the Thorax Using Iterative Reconstruction: Evaluation of Image Quality and Radiation Dose Reduction. AJR Am J Roentgenol 2015; 204: 1197-1202.
114) Yamada Y, Jinzaki M, Hosokawa T, Tanami Y, Sugiura H, Abe T, Kuribayashi S. Dose reduction in chest CT: Comparison of the adaptive iterative dose reduction 3D, adaptive iterative dose reduction, and filtered back projection reconstruction techniques. Eur J Radiol 2012; 81: 4185-4195.
115) Lee SW, Kim Y, Shim SS, Lee JK, Lee SJ, Ryu YJ, Chang JH. Image quality assessment of ultra low-dose chest CT using sinogram-affirmed iterative reconstruction. Eur Radiol. 2014; 24: 817-826.
116) Macri F, Greffier J, Pereira F, Rosa AC, Khasanova E, Claret PG, Larbi A, Gualdi G, Beregi JP. Value of ultra-low-dose chest CT with iterative reconstruction for selected emergency room patients with acute dyspnea. Eur J Radiol 2016; 85: 1637-1644.
117) Rawashdeh MA, Saade C. Radiation dose reduction considerations and imaging patterns of ground glass opacities in coronavirus: risk of over exposure in computed tomography. Radiol Med 2021; 126: 380-387.
118) Choo JY, Goo JM, Lee CH, Park CM, Park SJ, Shim MS. Quantitative analysis of emphysema and airway measurements according to iterative reconstruction algorithms: comparison of filtered back projection, adaptive statistical iterative reconstruction and model-based iterative reconstruction. Eur Radiol 2014; 24:799-806.
119) Sun J, Yu T, Liu J, Duan X, Hu D, liu Y, Peng Y. Image quality improvement using model-based iterative reconstruction in low dose chest CT for children with necrotizing pneumonia. BMC Med Imaging 2017; 17: 24.

120) Martin SP, Gariani J, Feutry G, Adler D, Karenovics W, Becker CD, Montet X. Emphysema quantification using hybrid versus model-based generations of iterative reconstruction: SAFIRE versus ADMIRE. Medicine 2019; 98: e14450.
121) Sun J, Yang L, Zhou Z, Zhang D, Han W, Zhang Q, Peng Y. Performance evaluation of two iterative reconstruction algorithms, MBIR and ASIR, in low radiation dose and low contrast dose abdominal CT in children. Radiol Med 125: 918-925.
122) Haubenreisser H, Meyer M, Sudarski S, Allmendinger T, Schoenberg SO, Henzler T. Unenhanced third-generation dual-source chest CT using a tin filter for spectral shaping at 100kVp. Eur J Radiol 2015; 84: 1608-1613.
123) Martini K, Higashigaito K, Barth BK, Baumueller S, Alkadhi H, Frauenfelder T. Ultralow-dose CT with tin filtration for detection of solid and sub solid pulmonary nodules: a phantom study. Br J Radiology 2015; 88: 20150389.
124) Martini K, Barth BK, Nguyen-Kim TDL, Baumueller S, Alkadhi H, Frauenfelder T. Evaluation of pulmonary nodules and infection on chest CT with radiation dose equivalent to chest radiography: Prospective intra-individual comparison study to standard dose CT. Eur J Radiol 2016; 85: 360-365.
125) Agostini A, Borgheresi A, Carotti M, Ottaviani L, Badaloni M, Floridi C, Giovagnoni A. Third-generation iterative reconstruction on a dual-source, high-pitch, low-dose chest CT protocol with tin filter for spectral shaping at 100 kV: a study on a small series of COVID-19 patients. Radiol Med 2021; 126: 388-398.
126) Vivier S, Deken V, Arous Y, Faivre JB, Duhamel A, Deschildre A, Flohr T, Remy J, Remy-Jardin M. Pediatric chest computed tomography at 100 kVp with tin filtration: comparison of image quality with 70-kVp imaging at comparable radiation dose. Pediatr Radiol 2020; 50: 188-198.
127) Leyendecker P, Faucher V, Labani A, Noblet V, Lefebvre F, Magotteaux P, Ohana M, Roy C. Prospective evaluation of ultra-low-dose contrast-enhanced 100-kV abdominal computed tomography with tin filter: effect on radiation dose reduction and image quality with a third-generation dual-source CT system. Eur Radiol 2019; 29: 2107-2116.
128) Seuss H, Janka R, Hammon M, Cavallaro A, Uder M, Dankerl P. Virtual Computed Tomography Colonography Evaluation of 2D and Virtual 3D Image Quality of Sub-mSv Examinations Enabled by Third-generation Dual Source Scanner Featuring Tin Filtering. Acad Radiol 2018; 25: 1046-1051.
129) Suntharalingam S, Mikat C, Wetter A, Guberina N, Salem A, Heil P, Forsting M, Nassenstein K. Whole-body ultra-low dose CT using spectral shaping for detection of osteolytic lesion in multiple myeloma. Eur Radiol 2018; 28: 2273-2280.
130) Nakaura T, Nakamura S, Maruyama N, Funama Y, Awai K, Harada K, Uemura S, Yamashita Y. Low Contrast Agent and Radiation Dose Protocol for Hepatic Dynamic CT of Thin Adults at 256–Detector Row CT: Effect of Low Tube Voltage and Hybrid Iterative Reconstruction Algorithm on Image Quality. Radiology 2012; 264: 445-454.
131) Pregler B, Beyer LP, Teufel A, Niessen C, Stroszczynski C, Brodoefel H, Wiggermann P. Low Tube Voltage Liver MDCT with Sinogram-Affirmed Iterative Reconstructions for the Detection of Hepatocellular Carcinoma. Sci Rep 2017; 7: 9460.
132) Nakamoto A, Yamamoto K, Sakane M, Nakai G, Higashiyama A, Juri H, Yoshikawa S, Narumi Y. Reduction of the radiation dose and the amount of contrast material in hepatic dynamic CT using low tube voltage and adaptive iterative dose reduction 3-dimensional. Medicine 2018; 97: e11857.
133) Yamamura S, Oda S, Utsunomiya D, Funama Y, Imuta M, Namimoto T, Hirai T, Chikamoto A, Baba H, Yamashita Y. Dynamic Computed Tomography of Locally Advanced Pancreatic Cancer. J Comput Assist Tomogr. 2013; 37: 790-796.
134) Noda Y, Kanematsu M, Goshima S, Kondo H, Watanabe H, Kawada H, Kawai N, Tanahashi Y, Miyoshi T, Bae KT. Reduction of Iodine Load in CT Imaging of Pancreas Acquired With Low Tube Voltage and an Adaptive Statistical Iterative Reconstruction Technique. J Comput Assist Tomogr 2014; 38: 714-720.
135) Kanematsu M, Goshima S, Kawai N, Kondo H, Miyoshi T, Watanabe H, Noda Y, Tanahashi Y, Bae KT. Low-Iodine-Load and Low-Tube-Voltage CT Angiographic Imaging of the Kidney by Using Bolus Tracking with Saline Flushing. Radiology 2015; 275: 832-840.
136) Kim SY, Cho JY, Lee J, Hwang SI, Moon MH, Lee EJ, Hong SS, Kim CK, Kim KA, Park SB, Sung DJ, Kim Y, Kim YM, Jung SI, Rha SE, Kim DW, Lee H, Shim Y, Hwang I, Woo S, Choi HJ. Low-Tube-Voltage CT Urography Using Low-Concentration-Iodine Contrast Media and Iterative Reconstruction: A Multi-Institutional Randomized Controlled Trial for Comparison with Conventional CT Urography. Korean J Radiol 2018; 19: 1119-1129.
137) Feng C, Zhu D, Zou X, Li A, Hu X, Li Z, Hu D. The combination of a reduction in contrast agent dose with low tube voltage and an adaptive statistical iterative reconstruction algorithm in CT enterography. Medicine 2018; 97: e0151.
138) Wang L, Gong S, Yang J, Zhou J, Xiao J, Gu J, Yang H, Zhu J, He B. CARE Dose 4D combined with sinogram-affirmed iterative reconstruction improved the image quality and reduced the radiation dose in low dose CT of the small intestine. J Appl Clin Med Phys 2018; 20: 293-307.
139) Goenka AH, Herts BR, Obuchowski NA, Primak AN, Dong F, Karim W, Baker ME. Effect of Reduced Radiation Exposure and Iterative Reconstruction on Detection of Low-Contrast Low-Attenuation Lesions in an Anthropomorphic Liver Phantom: An 18-Reader Study. Radiology 2014; 272: 154-163.
140) Goenka AH, Herts BR, Dong F, Obuchowski NA, Primak AN, Karim W, Baker ME. Image Noise, CNR, and Detectability of Low-Contrast, Low-Attenuation Liver Lesions in a Phantom: Effects of Radiation Exposure, Phantom Size, Integrated Circuit Detector, and Iterative Reconstruction. Radiology 2016; 280: 475-482.
141) Nam JG, Hong JH, Kim DS, Oh J, Goo JM. Deep learning reconstruction for contrast-enhanced CT of

the upper abdomen: similar image quality with lower radiation dose in direct comparison with iterative reconstruction. Eur Radiol 2021; 31: 5533-5543.
142) Marin D, Boll DT, Mileto A, Nelson RC. State of the art: dual-energy CT of the abdomen. Radiology 2014; 271: 327-342.
143) McCullough EC. Photon attenuation in computed tomography. Med Phys 1975; 2: 307-320.
144) Alvarez RE, Macovski A. Energy-selective reconstructions in X-ray computerized tomography. Phys Med Biol 1976; 21: 733-744.
145) Liu X, Yu L, Primak AN, McCollough CH. Quantitative imaging of element composition and mass fraction using dual-energy CT: three-material decomposition. Med Phys 2009; 36: 1602-1609.
146) Agostini A, Borgheresi A, Mari A, Floridi C, Bruno F, Carotti M, Schicchi N, Barile A, Maggi S, Giovagnoni A. Dual-energy CT: theoretical principles and clinical applications. Radiol Med 2019; 124: 1281-1295.
147) So A, Nicolaou S. Spectral Computed Tomography: Fundamental Principles and Recent Developments. Korean J Radiol 2021; 22: 86-96.
148) Palmisano A, Vignale D, Benedetti G, Maschio AD, Cobelli FD, Esposito A. Late iodine enhancement cardiac computed tomography for detection of myocardial scars: impact of experience in the clinical practice. Radiol Med 2020; 125: 128-136.
149) Parakh A, Lennartz S, An C, Rajiah P, Yeh BM, Simeone FJ, Sahani DV, Kambadakone AR. Dual-Energy CT Images: Pearls and Pitfalls. Radiographics 2021; 41: 98-119.
150) Rajiah P, Parakh A, Kay F, Baruah D, Kambadakone AR, Leng S. Update on Multienergy CT: Physics, Principles, and Applications. Radiographics 2020; 40: 1284-1308.
151) Almeida IP, Schyns LEJR, Öllers MC, Elmpt W van, Parodi K, Landry G, Verhaegen F. Dual-energy CT quantitative imaging: a comparison study between twin-beam and dual-source CT scanners. Med Phys 2017; 44: 171-179.
152) Rassouli N, Etesami M, Dhanantwari A, Rajiah P. Detector-based spectral CT with a novel dual-layer technology: principles and applications. Insights Imaging 2017; 8: 589-598.
153) Rajendran K, Petersilka M, Henning A, Shanblatt ER., Schmidt B, Flohr TG, Ferrero A, Baffour F, Diehn FE, Yu L, Rajiah P, Fletcher JG, Leng S, McCollough CH. First Clinical Photon-counting Detector CT System: Technical Evaluation. Radiology 2022; 303: 130-138.
154) Mileto A, Ananthakrishnan L, Morgan DE, Yeh BM, Marin D, Kambadakone AR. Clinical Implementation of Dual-Energy CT for Gastrointestinal Imaging. AJR Am J Roentgenol 2021; 217: 651-663.
155) Otrakji A, Digumarthy SR, Gullo RL, Flores EJ, Shepard JAO, Kalra MK. Dual-Energy CT: Spectrum of Thoracic Abnormalities. Radiographics 2016; 36: 38-52.
156) Digumarthy SR, Singh R, Rastogi S, Otrakji A, Homayounieh F, Zhang EW, McDermott S, Kalra MK. Low contrast volume dual-energy CT of the chest: Quantitative and qualitative assessment. Clin Imag 2021; 69: 305-310.
157) Wen Q, Yue Y, Shang J, Lu X, Gao L, Hou Y. The application of dual-layer spectral detector computed tomography in solitary pulmonary nodule identification. Quantitative Imaging Medicine Surg 2021; 11: 521-532.
158) Hong SR, Hur J, Moon YW, Han K, Chang S, Kim JY, Im DJ, Suh YJ, Hong YJ, Lee HJ, Kim YJ, Choi BW. Predictive factors for treatment response using dual-energy computed tomography in patients with advanced lung adenocarcinoma. Eur J Radiol 2018; 101: 118-123.
159) Lee CW, Seo JB, Lee Y, Chae EJ, Kim N, Lee HJ, Hwang HJ, Lim CH. A Pilot Trial on Pulmonary Emphysema Quantification and Perfusion Mapping in a Single-Step Using Contrast-Enhanced Dual-Energy Computed Tomography. Invest Radiol 2012; 47: 92-97.
160) Scharm SC, Vogel-Claussen J, Schaefer-Prokop C, Dettmer S, Knudsen L, Jonigk D, Fuge J, Apel RM, Welte T, Wacker F, Prasse A, Shin H oh. Quantification of dual-energy CT-derived functional parameters as potential imaging markers for progression of idiopathic pulmonary fibrosis. Eur Radiol 2021; 31: 1-12.
161) Ridge CA, Desai SR, Jeyin N, Mahon C, Lother DL, Mirsadraee S, Semple T, Price S, Bleakley C, Arachchillage DJ, Shaw E, Patel BV, Padley SP, Devaraj A. Dual-Energy CT Pulmonary Angiography (DECTPA) Quantifies Vasculopathy in Severe COVID-19 Pneumonia. Radiology Cardiothorac Imaging 2020; 2: e200428.
162) Holz JA, Alkadhi H, Laukamp KR, Lennartz S, Heneweer C, Püsken M, Persigehl T, Maintz D, Hokamp NG. Quantitative accuracy of virtual non-contrast images derived from spectral detector computed tomography: an abdominal phantom study. Sci Rep 2020; 10: 21575.
163) Marin D, Ramirez-Giraldo JC, Gupta S, Fu W, Stinnett SS, Mileto A, Bellini D, Patel B, Samei E, Nelson RC. Effect of a Noise-Optimized Second-Generation Monoenergetic Algorithm on Image Noise and Conspicuity of Hypervascular Liver Tumors: An In Vitro and In Vivo Study. AJR Am J Roentgenol 2016; 206: 1222-1232.
164) Caruso D, De Cecco CN, Schoepf UJ, Schaefer AR, Leland PW, Johnson D, Laghi A, Hardie AD. Can dual-energy computed tomography improve visualization of hypoenhancing liver lesions in portal venous phase? Assessment of advanced image-based virtual monoenergetic images. Clin Imag 2017; 41: 118-124.
165) Nakamura Y, Higaki T, Honda Y, Tatsugami F, Tani C, Fukumoto W, Narita K, Kondo S, Akagi M, Awai K. Advanced CT techniques for assessing hepatocellular carcinoma. Radiol Med 2021; 126: 925-935.
166) Hardie AD, Picard MM, Camp ER, Perry JD, Suranyi P, Cecco CND, Schoepf UJ, Wichmann JL. Application of an Advanced Image-Based Virtual Monoenergetic Reconstruction of Dual Source Dual-Energy CT Data at Low keV Increases Image Quality for Routine Pancreas Imaging. J Comput Assist Tomogr 2015; 39: 716-720.
167) Yu L, Leng S, McCollough CH. Dual-energy CT-based monochromatic imaging. AJR Am J Roentgenol 2012; 199: s9-s15.
168) Ascenti G, Sofia C, Mazziotti S, Silipigni S, D'Angelo T, Pergolizzi S, Scribano E. Dual-energy CT

with iodine quantification in distinguishing between bland and neoplastic portal vein thrombosis in patients with hepatocellular carcinoma. Clin Radiol 2016; 71: 938 e1-e9.
169) Yue X, Jiang Q, Hu X, Cen C, Song S, Qian K, Lu Y, Yang M, Li Q, Han P. Quantitative dual-energy CT for evaluating hepatocellular carcinoma after transarterial chemoembolization. Sci Rep-uk 2021; 11: 11127.
170) Werner S, Krauss B, Haberland U, Bongers M, Starke U, Bakchoul T, Enkel S, Nikolaou K, Horger M. Dual-energy CT for liver iron quantification in patients with haematological disorders. Eur Radiol 2019; 29: 2868-2877.
171) Hyodo T, Hori M, Lamb P, Sasaki K, Wakayama T, Chiba Y, Mochizuki T, Murakami T. Multimaterial Decomposition Algorithm for the Quantification of Liver Fat Content by Using Fast-Kilovolt-Peak Switching Dual-Energy CT: Experimental Validation. Radiology 2017; 282: 381-389.
172) Cicero G, Mazziotti S, Silipigni S, Blandino A, Cantisani V, Pergolizzi S, D'Angelo T, Stagno A, Maimone S, Squadrito G, Ascenti G. Dual-energy CT quantification of fractional extracellular space in cirrhotic patients: comparison between early and delayed equilibrium phases and correlation with oesophageal varices. Radiol Med 2021; 126: 761-767.
173) Martin SS, Trapp F, Wichmann JL, Albrecht MH, Lenga L, Durden J, Booz C, Vogl TJ, D'Angelo T. Dual-energy CT in early acute pancreatitis: improved detection using iodine quantification. Eur Radiol 2019; 29: 2226-2232.
174) Kaza RK, Ananthakrishnan L, Kambadakone A, Platt JF. Update of Dual-Energy CT Applications in the Genitourinary Tract. AJR Am J Roentgenol 2017; 208: 1185-1192.
175) Avesani G, Arshad M, Lu H, Fotopoulou C, Cannone F, Melotti R, Aboagye E, Rockall A. Radiological assessment of Peritoneal Cancer Index on preoperative CT in ovarian cancer is related to surgical outcome and survival. Radiol Med 2020; 125: 770-776.
176) Foti G, Mantovani W, Catania M, Avanzi P, Caia S, Zorzi C, Carbognin G. Evaluation of glenoid labral tears: comparison between dual-energy CT arthrography and MR arthrography of the shoulder. Radiol Med 2020; 125: 39-47.
177) Mileto A, Marin D. Dual-Energy Computed Tomography in Genitourinary Imaging. Radiol Clin N Am 2017; 55: 373-391.
178) Mallinson PI, Coupal TM, McLaughlin PD, Nicolaou S, Munk PL, Ouellette HA. Dual-Energy CT for the Musculoskeletal System. Radiology 2016; 281: 690-707.
179) Leng S, Shiung M, Ai S, Qu M, Vrtiska TJ, Grant KL, Krauss B, Schmidt B, Lieske JC, McCollough CH. Feasibility of Discriminating Uric Acid From Non–Uric Acid Renal Stones Using Consecutive Spatially Registered Low- and High-Energy Scans Obtained on a Conventional CT Scanner. AJR Am J Roentgenol 2015; 204: 92-97.
180) Bongartz T, Glazebrook KN, Kavros SJ, Murthy NS, Merry SP, Franz WB, Michet CJ, Veetil BMA, Davis JM, Mason TG, Warrington KJ, Ytterberg SR, Matteson EL, Crowson CS, Leng S, McCollough CH. Dual-energy CT for the diagnosis of gout: an accuracy and diagnostic yield study. Ann Rheum Dis 2015; 74: 1072.
181) Gosangi B, Mandell JC, Weaver MJ, Uyeda JW, Smith SE, Sodickson AD, Khurana B. Bone Marrow Edema at Dual-Energy CT: A Game Changer in the Emergency Department. Radiographics 2020; 40: 859-874.
182) Foti G, Mantovani W, Faccioli N, Crivellari G, Romano L, Zorzi C, Carbognin G. Identification of bone marrow edema of the knee: diagnostic accuracy of dual-energy CT in comparison with MRI. Radiol Med 2021; 126: 405-413.